CivilEng

MDPI

Article

Application of Graphene Oxide in Ordinary Concrete Materials: Modification and Performance Optimization

Lanying Xie [1,†], Haifan Wang [1,2,†], Ningbo Wang [1], Cheng Zhang [3], Xiangguo Li [3], Yang Lv [3] and Bo Tian [1,*]

[1] School of Energy and Power Engineering, Huazhong University of Science and Technology, Wuhan 430074, China
[2] China-EU Institute for Clean and Renewable Energy, Huazhong University of Science and Technology, Wuhan 430074, China
[3] State Key Laboratory of Silicate Materials for Architectures, Wuhan University of Technology, Wuhan 430070, China
* Correspondence: d202380567@hust.edu.cn
† These authors contributed equally to this work.

Abstract

Concrete, as a widely used construction material, suffers from performance degradation due to chloride penetration and sulfate attack in harsh environments. Conventional performance-enhancing methods are costly and emit high levels of carbon dioxide. This study modified graphene oxide (GO) with polycarboxylate superplasticizer (PCE) alone or PCE synergized with a rubber viscosity reducer, optimized dispersion (50 °C water bath for 1 h), and prepared C50 modified concrete (500 kg/m^3 cementitious materials, w/b = 0.33). GO contents were 0%, 0.001%, 0.003%, 0.005%; a group with 8% reduced cementitious materials (460 kg/m^3) was also tested. Results showed PCE-viscosity reducer synergy better dispersed GO, improving concrete workability. GO accelerated cement hydration via nucleation, refining C-S-H gel and reducing porosity. At 0.005% GO, 56 d drying shrinkage dropped by 29.3% vs. the blank, and 56 d chloride penetration electric flux was 586 C, meeting 100-year service life. Sulfate resistance also improved with higher GO content. Even with 8% less cementitious materials, modified concrete outperformed the blank. This provides support for GO's application in cement-based materials.

Keywords: graphene oxide (GO); concrete modification; dispersibility; durability; chloride ion penetration; sulfate attack

Check for updates

Academic Editors: Angelo Luongo and Aires Camões

Received: 27 November 2025
Revised: 9 February 2026
Accepted: 13 February 2026
Published: 26 February 2026

Copyright: © 2026 by the authors. Licensee MDPI, Basel, Switzerland. This article is an open access article distributed under the terms and conditions of the Creative Commons Attribution (CC BY) license.

1. Introduction

Cement-based materials are the most traditional and widely used building materials in today's society. As a typical representative, concrete materials are widely used in roads, bridges, houses, water conservancy and other engineering fields [1]. However, with prolonged service life, cement-based materials undergo varying forms and degrees of damage in diverse environments. Due to the cumulative destructive effects of multiple factors, the surface of the concrete structure becomes cracked, peeled off, broken or even disintegrated, causing serious impacts on buildings and greatly reducing their lifespan.

The erosion environment faced by western saline soil and marine engineering is more complicated. In recent years, it has been found that some marine concrete structures designed for the service life of 100 years have been corroded and damaged by seawater for more than 50% over a decade, resulting in a significant reduction in their service life [2]. Especially in seawater, which contains a large amount of sulfate and chloride ions [3], it can

accelerate the corrosion of steel bars and reduce the service life of concrete. In the saline soil areas of western China, buildings often encounter the destruction of sulfate ion erosion that sulfate enters the interior of cement stone through the pores and reacts with hydrated calcium silicate (C-S-H) and calcium hydroxide (CH) to produce corrosion products such as gypsum and ettringite (Aft) [4], causing the hydration products to decompose and lose their bonding properties. At present, improving the durability of concrete is still one of the current research hotspots. Therefore, improving concrete durability is crucial for the sustainable development of the cement and building-materials industry.

Research has been conducted on the poor durability of concrete, aiming to improve its strength and durability, reduce maintenance costs and extend its service life. Currently, there are mature application solutions available. For example, adding fibers to concrete can improve its mechanical properties, reduce shrinkage [5–7], and enhance its ability to resist splitting and fracture [8]. Appropriate cement varieties, concrete mix ratios, and lower water–cement ratios are selected based on the service environment of the building to enhance or improve the corrosion resistance of concrete [9–12]. The use of mineral admixtures with pozzolanic activity can increase the yield of hydration products and reduce the porosity of cement stone, thereby improving the resistance to salt ion erosion. However, improving the performance of concrete by adding cement, fiber or mineral admixtures is bound to increase the cost of concrete and consume a large amount of energy. In 2021, the global cement industry produced approximately 4.3 billion tons, consuming about 3% of the world's total energy consumption, and emitted approximately 2.6 billion tons of CO_2, accounting for about 7% of the world's total carbon emissions [13,14]. Researchers have found that producing one ton of cement clinker consumes approximately 52 kWh of electricity and emits 550 kg of carbon dioxide [15]. Additionally, the production process of concrete requires a large amount of cement and consumes a significant amount of electricity, which further exacerbates greenhouse gas emissions [16]. Therefore, exploring more energy-efficient and environmentally friendly ways to enhance the performance of cement-based materials is of great practical significance for prolonging their service life and reducing carbon emissions, and has become one of the current research hotspots.

Due to surface effects, dielectric confinement effects, volume effects, and quantum size effects, nanomaterials have shown wide applications in interdisciplinary fields, including biomedical, electronic devices, metals, coatings, building materials, and biosensing—a rapidly developing field that has recently made significant progress. Their unique physical and chemical properties, such as high specific surface area and adjustable surface functional groups, make them an ideal choice for high-sensitivity biosensors that can quickly detect biomolecules and pathogens. For example, Kurmendra [17] pointed out that 2D GO has superior biosensing sensitivity and polymer-mediated dispersion strategies, similar to PCE modification in this study. Lee et al. [18] developed a GO-CNT hybrid biosensor, in which 1D CNT reduced GO accumulation, providing a reference for optimizing the dispersion of GO in concrete.

The progress of these biosensing technologies highlights the core technological challenges faced by cement modification: dispersion control and surface functionalization. For example, the dispersion of GO induced by PEI in biosensors [17] is consistent with the strategy mediated by PCE, while GO surface groups [18] that promote the binding of biological receptors also promote the nucleation of C-S-H gel in cement.

In addition to biosensing, nanomaterials such as carbon nanotubes and nano silica have been explored for use in cement composites, but they face aggregation issues [19,20]. In contrast, the high aspect ratio and abundant functional groups of 2D GO make it more effective in microstructure refinement. The success of GO in biosensing further

confirms its potential in specific modification, bridging the gap in interdisciplinary research on nanomaterials.

Although nanomaterials can effectively improve various properties of cement-based composites, the impact of nanomaterials with different dimensions on their properties varies. Especially zero-dimensional nanomaterials, due to their low aspect ratio, lack the ability to capture and control nano-scale microcracks. The diameter of one-dimensional nanomaterials is relatively small, but its length can reach the centimeter level, making its aspect ratio exceed 1000 [21], which tends to agglomerate and has a negative impact on the performance of cement-based materials.

Reduced graphene oxide (rGO) lays the foundation for understanding the interaction between two-dimensional nanomaterials and C-S-H, which is consistent with the core mechanism explored in this study. Valizadeh Kiamahalleh et al. [22] experimentally demonstrated that rGO, with its surface epoxy and alkoxy functional groups, can serve as an effective heterogeneous nucleation site for C-S-H. It enhances the hydrophilicity of rGO, facilitating the penetration of water molecules into the cement micro-nano structure, thereby accelerating hydration and increasing the formation of C-S-H crystals. At the atomic scale, Aretxabaleta et al. [23] elucidated the role of rGO in C-S-H nucleation using DFT (density functional theory) and MD (molecular dynamics) simulations: rGO promotes the fusion of small silicate clusters into stable $C_4S_4H_2$ structural units, which crystallize into a dense, ordered C-S-H gel providing theoretical support for the nucleation mechanism observed in this study.

In addition to nucleation, the groundbreaking first principle study further revealed the basic interaction mechanism between rGO and C-S-H gel: Izadifar et al. [24] systematically studied the combination of hydroxyl/epoxy functionalized rGO with C-S-H monomer through DFT calculation, and found that hydroxyl rGO can selectively repair lattice defects and form water molecules through condensation reaction, while epoxy rGO maintains structural stability at the interface—the coulomb interaction driven by charge transfer dominates the rGO-C-S-H bonding. At the same time, Izadifar et al. [25] reported the first experimental evidence of enhancing the elastic properties of C-S-H by inserting rGO, indicating that hydroxyl rGO modified snow silicate limestone has significantly increased bulk modulus compared to pure C-S-H.

Furthermore, Zhang et al. [26] demonstrated that the two-dimensional morphology and nucleation effect of rGO synergistically refine the microstructure of C-S-H: the formation of a cross-linked C-S-H network reduces porosity and increases the compressive strength of mortar from 55 MPa to 71 Mpa, while the flexural strength is improved by 49% and the elastic modulus is significantly enhanced. Despite these pioneering contributions, research based on rGO still faces key limitations in engineering applications: (1) rGO requires an energy-intensive reduction process, leading to higher costs and greater environmental impact; (2) the low oxygen content of rGO reduces its dispersibility in high-alkalinity, high-Ca^{2+} cement pastes, exacerbating agglomeration; (3) most studies focus on laboratory-scale cement pastes or mortars, with limited data on full-scale concrete (including aggregates) or scenarios involving reduced cementitious materials [26].

In contrast, this study extends the pioneering mechanism of rGO-C-S-H interaction to more cost-effective and engineerable GO, and validates its performance in real concrete formulations. GO is a highly complex two-dimensional nanomaterial with high elastic modulus and tensile strength, and the aspect ratio of a single GO layer can theoretically reach over 2000 [27]. Compared with zero-dimensional and one-dimensional nanomaterials, the larger surface area exposed by GO sheets provides more potential sites for favorable chemical or physical interactions, which in turn improves the bonding between GO layers and host materials. Therefore, it has been highly favored by researchers [28].

Researchers have found that the incorporation of GO into cement-based materials can improve their multiple properties [29]. Therefore, as an admixture in cement-based materials to enhance their various properties, GO has gradually become a research hotspot in the cement building-materials industry.

It is noteworthy that there are fundamental differences between GO and rGO in terms of interfacial bonding and mechanical reinforcement. Unlike rGO, which mainly relies on physical adsorption and interaction with C-S-H, GO retains abundant carboxyl and hydroxyl groups, which can chelate with Ca^{2+} in cement paste and form stable chemical–physical dual bonding with hydration products. In addition, GO exhibits excellent dispersibility due to the inherent electrostatic repulsion of its ionized carboxyl groups, avoiding severe agglomeration of rGO in highly alkaline cement paste [26], thus achieving uniform reinforcement and consistent pore refinement, which are key advantages in engineering applications.

At present, many researchers have conducted extensive research on the application of GO in cement-based materials, and the effects on cement-based materials vary. Firstly, it is found that GO can effectively improve the strength and durability of cement-based materials. Research has found that GO can effectively improve the strength and durability of cement-based materials [30,31]. Devi et al. [32] studied the effect of GO content on the mechanical and impermeability properties of concrete. It was found that when the GO content was 0.08%, the compressive strength increased the most, and the permeability decreased with the increase in GO content. Zhu et al. [21] used GO to prepare cement-based composites and found that when the GO content was 0.05%, the compressive strength could be increased by more than 15%, and the flexural strength could be increased by more than 40%.

GO can establish effective nucleation sites for cement, promote hydration process, and affect the crystal form of hydration products to improve the pore structure. Lin et al. [33] analyzed the effect of GO on the hydration process of cement, and found that GO could provide adsorption sites and nucleation sites for cement and water, which significantly accelerated the hydration rate of cement. Li et al. [34] found that the incorporation of GO into cement-based materials can effectively reduce the porosity of cement paste and improve mechanical properties. At the same time, it can also promote the dissolution of C_3A (tricalcium aluminate), increase the rate of the second exothermic peak of hydration and increase the total amount of hydration heat release. Lv et al. [35] used a scanning electron microscope (SEM) to study the effect of GO on the microstructure of cementation products. They found that GO can promote the formation of dense flower-shaped crystals in hydration crystals. These flower-like crystals can fill the pores and cracks of cement stone and produce cross-linking, so as to realize the refinement of pore structure and the reduction in porosity.

Although GO has excellent dispersibility in water, it is still unstable and easy to agglomerate in cement-based materials due to its small particle size and large specific surface area, resulting in a significant reduction in its nano-enhancement effect. It has been reported that due to the high pH and the high content of Ca^{2+} in the cement paste, GO, which is well-dispersed in aqueous solution, will chelate and cross-link with Ca^{2+} in the cement paste after being added to the cement paste [36]. Wu et al. [37] studied the aggregation behavior of GO in water through molecular dynamics simulation. They found that GO undergoes deprotonated when dissolved in water, and the electrostatic repulsion between the ionized carboxyl groups at the edges enabled GO to disperse well. When divalent cations enter, they will cross-link with GO, providing additional shielding for the charged surface to reduce the electrical repulsion between particles, thereby promoting their aggregation. Chowdhuryet al. [38] studied the effects of pH and ion concentration

on the aggregation and stability of GO. The results showed that the presence of divalent ions (Ca^{2+}, Mg^{2+}) significantly reduced the stability of GO and induced agglomeration at high pH, leading to a decrease in stability. Liet al. [39] found that the addition of GO that is well-dispersed in the aqueous solution to the cement paste will cause agglomeration, which will reduce the working performance of the cement paste, resulting in no significant improvement in the hydration of cement by GO and a decrease in the reinforcement and toughening effect. Therefore, solving the agglomeration problem of GO in cement paste is the core key to realize its widespread application in cement-based materials.

Therefore, considering that ordinary concrete is susceptible to chloride ion penetration and sulfate attack in complex service environments, resulting in attenuation of mechanical properties and shortened service life. At the same time, the traditional schemes to improve the performance of concrete have problems such as high cost and large carbon emissions. To improve the mechanical properties and durability of concrete, this study uses polycarboxylate superplasticizer (PCE) and rubber reducer to modify GO, and prepared modified concrete materials by optimizing the dispersion process. The effects of GO dispersion on the mechanical properties, volume stability and durability of concrete were studied, which provided theoretical and experimental support for the application of GO in cement-based materials.

2. Materials and Methods

2.1. Materials

2.1.1. Gel Material

The cement used in this study is P.O 42.5 ordinary Portland cement produced by Huaxin building materials group Co., Ltd. (Huangshi, China), with a median particle size (D50) of 10.81 μm and a bulk density of 3150 kg/m^3. The S95 grade mineral powder and I grade fly ash used in this study were purchased from Wuhan VCEM Technology Development Company Limited (Wuhan, China). The D50 of mineral powder is 12.53 μm, and the bulk density is 2850 kg/m^3. The median particle size of fly ash is 13.84 μm and the bulk density is 2400 kg/m^3. The chemical compositions are presented in Table 1, and the results of particle-size analysis are illustrated in Figure 1.

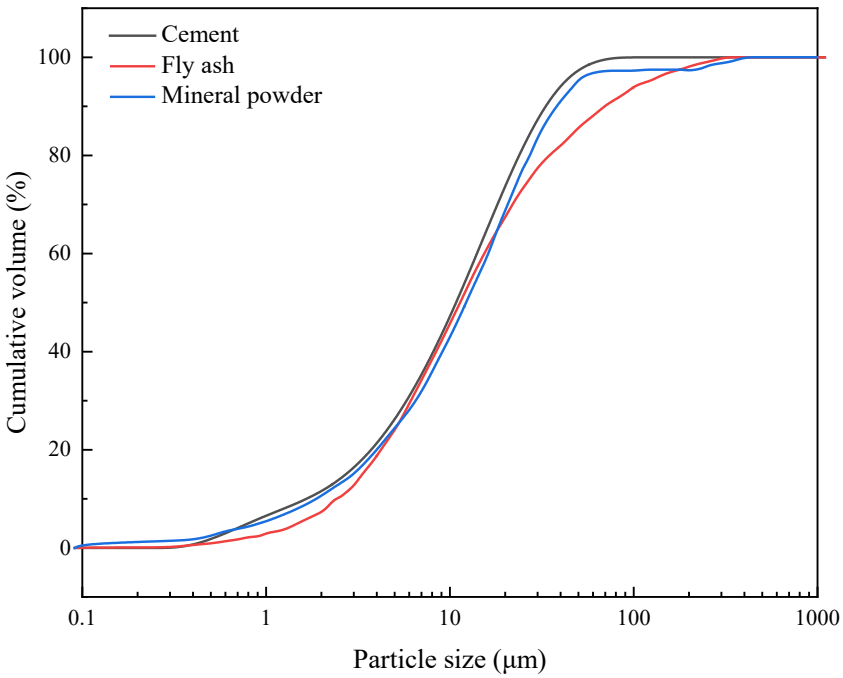


Figure 1. Particle-size analysis of raw materials.

Table 1. Chemical composition of raw materials.

Materials	Chemical Composition/%								
	CaO	SiO_2	Al_2O_3	Fe_2O_3	MgO	SO_3	K_2O	Na_2O	Other
Cement	57.61	23.23	6.83	3.30	1.81	2.44	1.07	0.27	3.44
Mineral powder	36.82	26.75	19.66	0.32	11.10	2.65	0.29	0.84	1.20
Fly ash	3.70	47.70	37.53	4.55	0.94	1.04	1.62	0.60	2.32

2.1.2. GO

The monolayer graphene oxide (GO) dispersion used in this study was purchased from a company in Hangzhou, China, with a concentration of 10 mg/g and a solid content of 1%. Its appearance is a uniform dark brown emulsion (Figure 2a), indicating good colloidal stability in aqueous solution. To systematically characterize the morphological, structural, and chemical properties of GO, multiple characterization techniques including Scanning Electron Microscopy (SEM) and X-ray Diffraction (XRD) were employed, with detailed test parameters and procedures as follows:

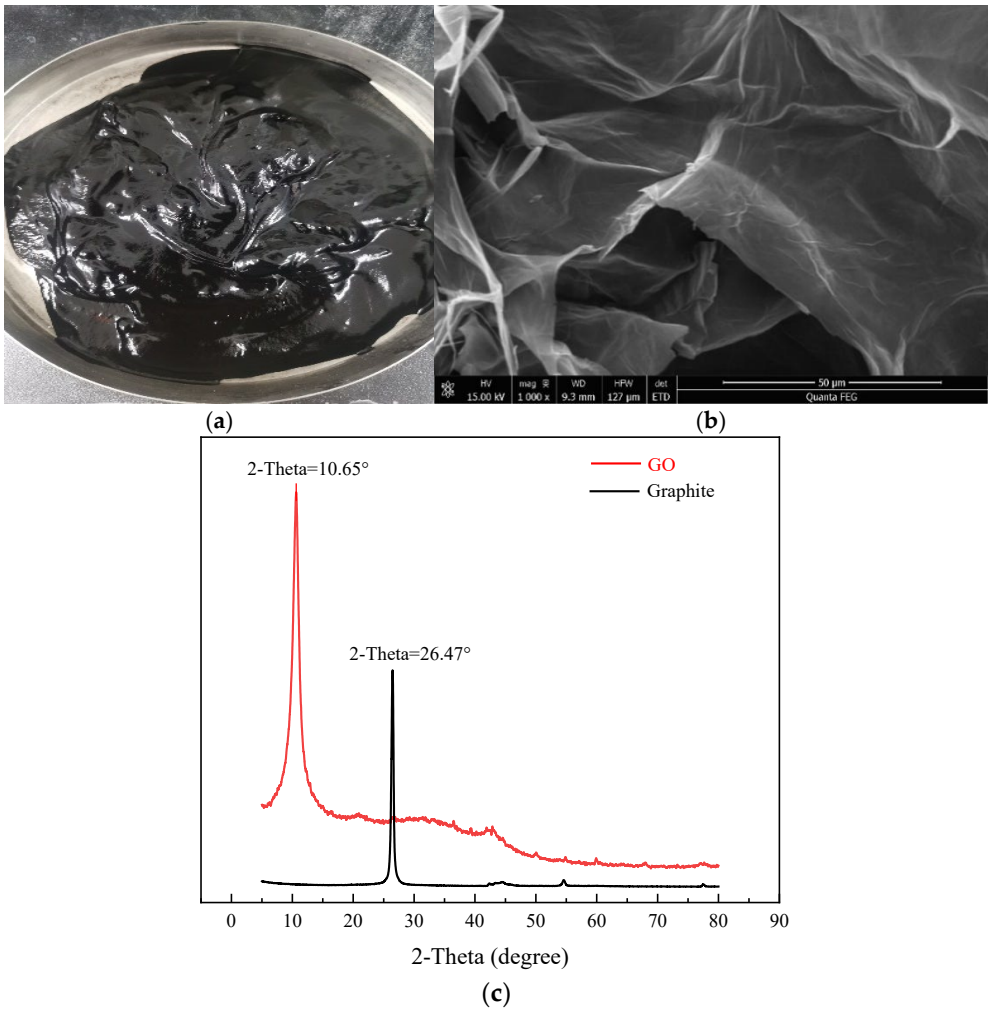


Figure 2. (**a**) Appearance of monolayer GO (**b**) SEM image of GO (**c**) XRD spectra of GO.

Scanning Electron Microscopy (SEM) observations were performed using a Quanta FEG 250 field-emission scanning electron microscope (FEI, Hillsboro, OR, USA) to analyze the morphological features of GO. Sample preparation: The as-received GO dispersion was first subjected to vacuum freeze-drying at −50 °C for 24 h to remove residual water—this

method avoids agglomeration caused by surface tension during air-drying, ensuring the preservation of the original lamellar structure. The dried GO powder was then mounted on a sample stage using conductive adhesive and sputter-coated with a 5 nm thick gold layer to enhance electrical conductivity (preventing charge accumulation under electron beam irradiation). Test parameters: The acceleration voltage was set to 15.00 kV (as indicated in Figure 2b caption), and images were captured at a working distance (WD) of 9.3 mm with a magnification of 1000×.

As shown in Figure 2b, the freeze-dried GO exhibits a typical two-dimensional (2D) lamellar structure with a large lateral dimension (estimated to be 1–5 μm) and abundant surface wrinkles. These wrinkles are attributed to the introduction of oxygen-containing functional groups (e.g., carboxyl (-COOH), hydroxyl (-OH)) during the strong oxidation of graphite: the intercalation of oxygen and hydrogen atoms between graphite layers disrupts the ordered hexagonal lattice, leading to interlayer expansion and sheet curling during drying. This wrinkled lamellar structure significantly increases the specific surface area of GO, which is crucial for providing sufficient active sites for interfacial interactions with cement hydration products (e.g., C-S-H gel) in subsequent concrete preparation.

X-ray Diffraction (XRD) analysis was conducted using a D8 Advance X-ray diffractometer (Bruker, Walzbachtal, Germany) to investigate the crystal structure and oxidation degree of GO. Test parameters: The radiation source was Cu Kα (λ = 0.15406 nm), operating at 40 kV and 40 mA. The scanning range was 2θ = 5–50°, with a scanning speed of 5°/min and a step size of 0.02° to ensure high-resolution data collection. For comparison, pristine graphite powder (the raw material of GO) was also tested under the same conditions.

As presented in Figure 2c, the pristine graphite shows a sharp and intense characteristic peak at 2θ = 26.47°, corresponding to the (002) crystal plane of graphite. According to the Bragg equation ($2d\sin\theta = n\lambda$, where $n = 1$), the interlayer spacing (d_{002}) of graphite is calculated to be 0.336 nm, which is consistent with the theoretical value of graphite's layered structure and reported in recent studies [24,40]. Yalovega et al. [40] confirmed that the (002) peak of pristine graphite typically appears at 2θ = 26.4–26.6° with an interlayer spacing of ~0.335–0.337 nm, validating the purity of our graphite raw material.

In contrast, the GO sample exhibits a distinct characteristic peak at 2θ = 10.65°, which shifts significantly to a lower 2θ angle—indicating a marked expansion of the interlayer spacing to 0.830 nm. This expansion is a direct result of the intercalation of oxygen-containing functional groups and adsorbed water molecules between the graphite layers during oxidation, which weakens the van der Waals forces between adjacent layers and achieves effective exfoliation. Consistent with our results, Yalovega et al. [40] reported that high-quality monolayer GO exhibits a characteristic (001) peak at 2θ = 10.5–10.8° with an interlayer spacing of 0.82–0.84 nm, while Wang et al. [41] further verified that the absence of the graphite (002) peak confirms complete oxidation.

Notably, no characteristic peak of pristine graphite (2θ = 26.47°) is detected in the XRD pattern of GO, confirming that the graphite raw material was fully oxidized and no unoxidized graphite residues remain. Additionally, the GO characteristic peak (2θ = 10.65°) is broader than that of graphite, which reflects a decrease in crystallinity due to the structural disorder introduced by oxidation this is consistent with the presence of abundant functional groups and wrinkled lamellar morphology observed in SEM.

The combined SEM and XRD results verify that the purchased GO possesses the typical structural features of high-quality monolayer GO: a large specific surface area, abundant oxygen-containing functional groups, and complete oxidation—laying a foundation for its effective dispersion in cement paste and interaction with hydration products.

2.1.3. Other Materials

The coarse aggregate used in this study is a continuously graded gravel from a commercial concrete company in Wuhan, China with a nominal particle size of 5–30 mm, tan apparent density of 2760 kg/m^3, a bulk density of 1650 kg/m^3, and a mud content of less than 1.1%. The fine aggregate used in this study is ISO standard sand that meets the requirements of 'Test method of cement mortar strength (ISO method) (GB/T 17671-2021 [42]), with a bulk density of 1600 kg/m^3. The superplasticizer used in this study is high-efficiency polycarboxylate superplasticizer (PCE) with a density of 1080 kg/m^3 and a solid content of 20%. The molecular formula of polycarboxylate superplasticizer is shown in Figure 3, with a density of 1020 kg/m^3. The reagents such as NaCl, Na_2SO_4 and NaOH used in this study were purchased from Sinopharm Chemical Reagent Co., Ltd. (Shanghai, China), and are all analytically pure. The concrete reducing agent used comes from a company in Wuhan, with a solid content of 5%. The main components are diethanol monoisopropanolamine (85%) and triethanolamine, with a reducing rate greater than 5%. The sand used for preparing mortar is ISO Chinese standard sand.

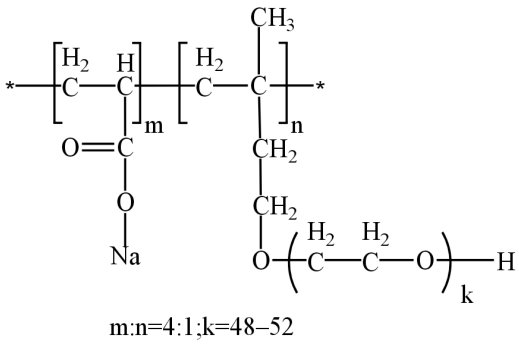


Figure 3. Molecular formula of polycarboxylate superplasticizer.

2.2. Mix Ratio Design

All mix ratios are designed using the volumetric mass combination method according to JGJ55-2011 [43], which prioritizes the density characteristics of raw materials to ensure the volumetric compatibility and target volumetric density (2450 kg/m ^{3}) of C50 concrete.

2.2.1. Optimization of GO Cooperative Dispersion System

The synergistic dispersion of GO was achieved by using PCE and a defoaming agent in combination. Initially, PCE and GO were mixed at mass ratios of 1:1, 3:1, and 5:1, respectively. Subsequently, the three components were mixed and dispersed according to the mass ratio of GO to defoaming agent at 1:1, 1:3, and 1:6, with the dispersions designated as X, Y, and Z, respectively. Dispersion was achieved by ultrasonication for 10 min and 20 min, and heating and stirring in a water bath at 50 °C for 1 h and 2 h, respectively. After reaching the set time, the dispersions were taken out, allowed to stand for 5 min, and then tested using a UV-Vis spectrophotometer.

Observe Figure 4 for the effect of the combined addition of deflocculant and PCE on the absorbance of the GO solution. The abscissa in the figure represents the mass ratio of GO to deflocculant. The control group was prepared by mixing the solution evenly and then leaving it at room temperature without any further treatment. It can be observed that the addition of deflocculant to the PCE and GO solution increases its absorbance. Furthermore, as the amount of deflocculant increases, the dispersibility of the solution gradually improves, indicating that the deflocculant promotes the dispersion of GO. The synergistic dispersion of GO by PCE and deflocculant is more effective than the dispersion

by a single component. When the ratio of PCE/GO is 5:1, the dispersibility of the solution is optimal.

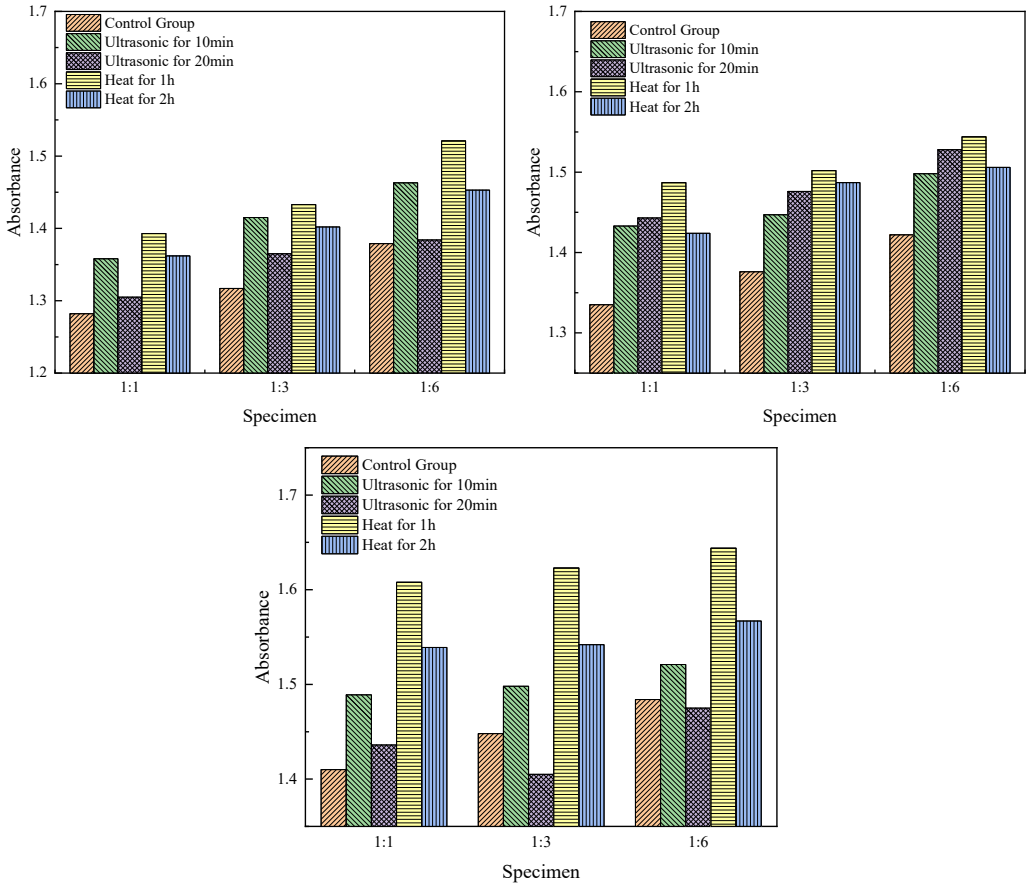


Figure 4. The influence of compounding PCE with a rubber reducing agent on the dispersion effect of GO.

2.2.2. Mix Ratio Design of Ordinary Concrete

Prepare C50 ordinary concrete specimens, and design the mix ratio according to JGJ55-2011 [43]. After referring to the design results of numerous researchers [44–46], the following ratio is designed according to the needs of this study, the total amount of cementitious material is 500 kg, including cement, mineral powder and fly ash. The water–binder ratio is 0.33, and the sand ratio is 39%. The content of GO is set at 0%, 0.001%, 0.003% and 0.005% of the total mass of cementitious materials, and each group is compiled as CG-0, CG-1, CG-2 and CG-3, accordingly. In this study, the dispersion method of water bath heating at 50 °C and constant temperature for 1 h was used to mix the materials according to the mass ratio of PCE to GO of 5:1. Simultaneously, the mortar in the concrete is used for drying shrinkage and autogenous shrinkage tests, with the specific mix ratio as shown in Table 2.

Table 2. Ratio of concrete (Unit: kg/m^3).

Samples	GO/%	Cement	Mineral Powder	Fly Ash	Gravel	Sand	Water	PCE
CG-0	0	320	120	60	1050	668	165	2.7
CG-1	0.001	320	120	60	1050	668	165	2.7
CG-2	0.003	320	120	60	1050	668	165	3
CG-3	0.005	320	120	60	1050	668	165	3.3

2.2.3. Mix Ratio Design of GO Compound Reducing Agent

To explore the effect of GO dispersion mixed with reducing agent on the performance of concrete, a reducing agent with a total amount of 0.6% of cementitious material was added based on the recommended amount of glue reducer. In order to maintain the consistency of economy and strength grade of the concrete after adding the reducing agent, the cementitious material was reduced by 8%, the sand ratio was increased and the amount of sand and gravel was increased while ensuring the constant water demand. The main component of the reducing agent solvent is water, so all the reducing agent are regarded as mixing water and included in the total water consumption. GO dispersion was heated in water bath at 50 °C and kept at that temperature for 1 h. The mass ratio of reducing agent/PCE/GO was 6:5:1, and the corresponding group numbers were C-0 (GO content 0%, cementitious material 500 kg/m^3), C-1 (GO content 0.001%, cementitious material 500 kg/m^3), C-2 (GO content 0.003%, cementitious material 500 kg/m^3), C-3 (GO content 0%, cementitious material 460 kg/m^3), C-4 (GO content 0.001%, cementitious material 460 kg/m^3), and C-5 (GO content 0.003%, cementitious material 460 kg/m^3). The specific mix ratios are shown in Table 3. To distinguish the independent effect of GO from the increased water–cement ratio, Group C-3 was designed as the baseline, which had the same water–cement ratio and mixing parameters as Groups C-4 and C-5, thus ensuring that the performance differences between C-4/C-5 and C-3 were solely attributed to graphene oxide.

Table 3. Concrete mix ratios of GO compound reducing agent (Unit: kg/m^3).

Samples	GO/%	Cement	Mineral Powder	Fly Ash	Gravel	Sand	Water	Cementitious Materials Reducing Agent	PCE
C-0	0	320	120	60	1050	668	162	3	2.7
C-1	0.001	320	120	60	1050	668	162	3	2.7
C-2	0.003	320	120	60	1050	668	162	3	2.7
C-3	0	290	110	60	1080	691	162.3	2.76	3
C-4	0.001	290	110	60	1080	691	162.3	2.76	3.1
C-5	0.003	290	110	60	1080	691	162.3	2.76	3.2

2.3. Test Methods

2.3.1. Slump Test

Weigh the materials according to the mix ratio, put them into the horizontal concrete forced mixer, start the mixer to stir the raw materials evenly, then add water and GO dispersion evenly and stir for 3 min. Pour the mixed concrete out of the mixer and use the cone bucket method to test the slump and expansion of the concrete. During the test, the mixed concrete was divided into three parts and loaded into the cone bucket. Each time, a vibrator was inserted into the center of the bucket 25 times along the wall of the bucket. When inserting, it needed to penetrate to the surface of the next layer. Finally, the concrete at the mouth of the bucket was flattened, and the cone bucket was lifted vertically. When the concrete collapsed naturally, the slump and expansion were measured. After the test was completed, the concrete was loaded into a 100 mm × 100 mm × 100 mm cube mold and compacted. After 24 h, it was demolded and placed in a standard curing room (temperature 20 ± 2 °C, relative humidity ≥ 95%) for curing to a specified age for subsequent mechanical performance testing.

2.3.2. Autogenous Shrinkage Test

Referring to the standard for test methods of long-term performance and durability of concrete (GB/T 50082-2024 [47]), the development law of concrete autogenous shrinkage was measured by bellows autogenous shrinkage tester. A bellows with diameter of 420 ± 5 mm and inner diameter of 29 mm was used as the specimen mold, and the test tem-

perature was controlled at 20 ± 2 °C. After stirring the mortar, load it into the bellows, and then immediately install it on the testing instrument. Set the instrument to automatically sample once every 5 min with a test accuracy of 1 μm and a total test time of 7 days.

2.3.3. Dry Shrinkage Test

The drying shrinkage test was carried out according to the standard test method for drying shrinkage of mortar (JC/T 603-2004 [48]). The specimen was demolded after 24 h of molding, and the initial length of the specimen was measured after 2 days of curing in the standard curing room. Then, the specimen was transferred to a curing box with a temperature of 20 ± 2 °C and a relative humidity of 55 ± 5%. The length of the specimen was measured, and the length variation was calculated at 1 d, 3 d, 7 d, 14 d, 21 d, 28 d, 42 d and 56 d, respectively. Measure the length of the specimen using a length gauge and record the reading of the length gauge to the nearest 0.001 mm.

2.3.4. Sulfate Resistance Test

Two sets of specimens with the same mix of concrete were prepared for the same specifications and cured in a standard curing room for 28 days. Then, they were soaked in water and 5% $NaSO_4$ solution, respectively, with erosion ages of 28 d, 56 d and 90 d, respectively. After reaching each erosion age, take out the specimens and dry the surface. Use a pressure testing machine to test the compressive strength, and calculate its corrosion resistance coefficient according to Formula (1) to evaluate the sulfate resistance of concrete:

$$K_f = \frac{f_{cn}}{f_{c0}} \times 100\% \quad (1)$$

In this formula, K_f is the corrosion resistance coefficient. f_{cn} is the measured compressive strength of a group of concrete specimens immersed in sulfate attack solution, in MPa. f_{c0} is the compressive strength of a group of contrast concrete specimens with the same age of sulfate attack specimens, in MPa.

2.3.5. Anti-Chloride Ion Penetration Test

The resistance to chloride ion penetration of concrete was tested by the electric flux method. Prepare 3 cylindrical specimens with a diameter of 100 mm × 50 mm, and cure them in a standard curing room for 28 d and 56 d. Seal the sides of the specimens, and place them in an electric flux testing device. Inject 3% NaCl solution (negative electrode) and 0.3 mol/L NaOH solution (positive electrode) on both sides of the specimens, apply a DC voltage of 60 V, and measure the total electric flux (C) passing through the specimen after 6 h of curing. The final electric flux value of each group is the average of the three parallel specimens. The smaller the electric flux, the stronger the resistance of concrete to chloride ion penetration.

3. Results and Discussion

3.1. Slump and Expansion Analysis

The working performance of concrete directly affects its construction convenience and forming quality. Slump and expansion are the core indexes to evaluate the workability.

Table 4 shows the test results of slump and expansion of CG series concrete. According to the table, the flowability of concrete decreased significantly after the incorporation of GO solution. In order to ensure the workability of concrete, the amount of water reducing agent was appropriately increased on the basis of ordinary mix ratio in the design of concrete mix ratio to ensure good working performance. From the table, it can be found that with the increase in GO dispersion content, the expansion and slump of concrete gradually decrease. Finally, the slump of each group of concrete maintained within the range of 208 ± 10 mm,

and the expansion degree maintained within the range of 550 mm, all of which meet the workability requirements of C50 concrete in the standard for test method of performance on ordinary fresh concrete.

Table 4. Concrete slump and expansion/mm.

Index	CG-0	CG-1	CG-2	CG-3
Expansion	570	565	556	535
Slump	223	218	213	208

When using the GO solution dispersed with PCE and reducing agent to prepare concrete, the water consumption should be controlled to be the same. This is because reducing the amount of cementitious material is equivalent to increasing the water–binder ratio. In order to ensure the consistency of concrete workability and strength grade, it is necessary to increase the amount of sand and gravel, which is equivalent to increasing the sand ratio. The reasonable ratioing parameters should be determined through multiple experiments, and the slump of concrete should be controlled within the range of 210 ± 10 mm, and the expansion degree should be about 550 mm × 560 mm. Its performance meets the requirements of GB/T50080-2016 [49].

The effect of GO dispersed by PCE synergistic reducing agent on the workability of concrete is shown in Table 5. Observing the data in the table, it can be found that when the GO dosage is the same, the workability of the experimental group CG-0, CG-1, CG-2 compared to C-0, C-1, C-2 is better when using PCE compounded and reducing agent dispersed GO solution to prepare concrete than when using PCE dispersed GO solution alone. There are two main reasons for this phenomenon: one is that the synergistic effect of PCE and reducing agent can significantly improve the dispersibility of GO in cement slurry, reducing the agglomeration of GO in cement slurry. On the other hand, the main components of PCE and reducing agent belong to surfactants. When PCE and reducing agent enter the cement slurry, they can be adsorbed onto the surface of cement particles, break the flocculent structure formed by cement particles, release the encapsulated free water, reduce the dislocation resistance of cement particle dispersion, and improve the fluidity of the slurry.

Table 5. The influence of PCE synergistic reducing agent dispersed GO on the workability of concrete/mm.

Index	C-0	C-1	C-2	C-3	C-4	C-5
Expansion	575	570	560	580	570	535
Slump	225	220	214	230	225	220

3.2. Autogenous Shrinkage

Autogenous shrinkage refers to the self-drying shrinkage of cement-based materials, which occurs when the cement gradually consumes the free water in the internal pores and hardens under closed conditions without exchanging water with the external environment. This results in a decrease in relative humidity and an increase in the shrinkage force of the capillary pores inside the material. Due to the water–binder ratio of ordinary concrete being lower than 0.4 and the use of a large number of cementitious materials, the early autogenous shrinkage will change greatly. Autogenous shrinkage mainly continues to develop after the final setting of cement, and there will be a significant volume change before the final setting of cement, mainly caused by chemical shrinkage, which is generally not considered in the study of autogenous shrinkage. Therefore, the test results of autogenous shrinkage are generally begin to be calculated after the final setting.

As shown in Table 6, with the increase in GO content, the final setting time of concrete gradually shortens, and the more GO content, the shorter the final setting time. This is because the nucleation effect of GO accelerates the hydration process of C3S and C3A in cement, and GO also reduces the workability of concrete, ultimately leading to the shortening of the setting time. When using the GO solution co-dispersed with PCE and reducing agent, the well-dispersed GO solution has a more significant effect on the hydration process of cement, further shortening the final setting time.

Table 6. The influence of different GO contents on setting time.

Samples	CG-0	CG-1	CG-2	CG-3
Final setting time (min)	267	253	233	201

The effect of different GO content on the autogenous shrinkage of concrete is shown in Figure 5. With the increase in GO content, the autogenous shrinkage showed a trend of first decreasing and then increasing, and the autogenous shrinkage change rate was the highest within 15 h after the final setting. The autogenous shrinkage values of each group were 284 μm/m and 286 μm/m, respectively, which were 24.1−24.6% lower than that of CG-0 (374 μm/m). This may be due to the fact that GO has a large tensile strength, and its nucleation effect can promote the formation of hydration products, refine the morphology of C-S-H gel and compact the microstructure, while inhibiting the shrinkage of capillary pores and reducing the volume deformation. When the content of GO increases to 0.005%, GO tends to agglomerate in the highly alkaline environment of cement slurry and adsorbs a large amount of water, resulting in a decrease in the equivalent water–binder ratio of the slurry and an increase in autogenous shrinkage.

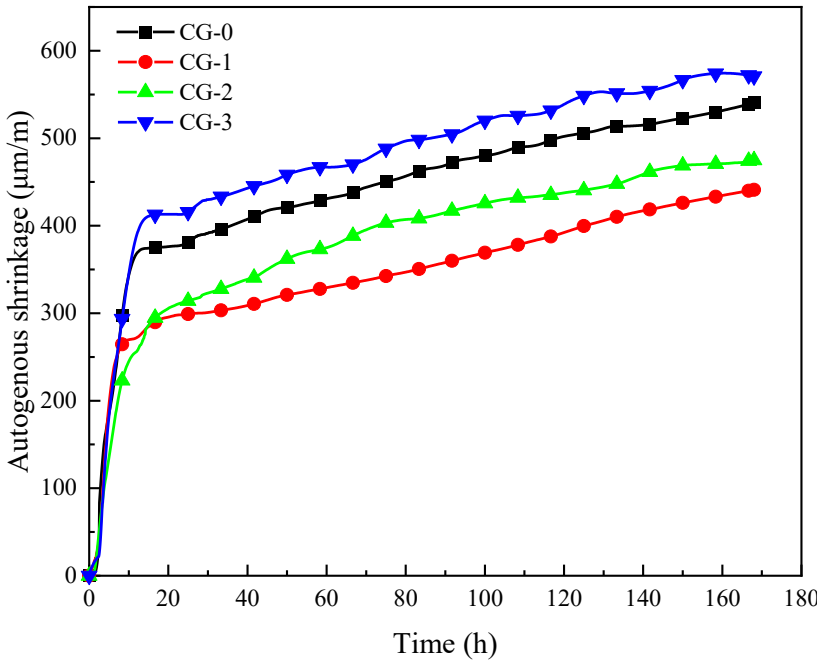


Figure 5. The influence of different GO contents on the autogenous shrinkage of concrete.

Table 7 shows the effect of PCE blended reducing agent dispersing GO on the final setting time. Comparing C-0, C-1, C-2 (cementitious material 500 kg/m^3) with CG-0, CG-1 and CG-2, it can be found that the final setting time of concrete was slightly shortened after the addition of the reducing agent. This is because the amine components in the reducing agent can accelerate the hydration of C_3A and produce a synergistic hydration effect with

GO. By comparing C-3, C-4, C-5 (cementitious material 460 kg/m^3) with C-0, C-1, C-2, it can be found that the final setting time of concrete was significantly prolonged after reducing the amount of cementitious material. This is because reducing the amount of cementitious material without reducing water consumption is equivalent to increasing the water–binder ratio. Moreover, due to the synergistic dispersion effect of PCE and reducing agent, it can break the flocculent agglomeration between cement particles, improve the workability of concrete, and ultimately lead to an increase in the final setting time.

Table 7. The influence of GO dispersed by PCE synergistic reducing agent on setting time/min.

Samples	C-0	C-1	C-2	C-3	C-4	C-5
Final setting time (min)	251	240	225	260	251	230

Figure 6 shows the effect of different GO content on the autogenous shrinkage of concrete. Since the dispersion of GO by PCE synergistic reducing agent can improve the strength of concrete and accelerate its hydration, its autogenous shrinkage is also increasing. The experimental group C-0 only added the reducing agent but did not reduce the amount of cementitious material used, which did not significantly promote hydration. Therefore, its autogenous shrinkage was comparable to that of the control group. Observing experimental groups C-3 and C-4, when reducing the amount of cementitious material, due to the increase in the equivalent water–binder ratio, there was more free water in the pores during the hardening of the slurry, which increased the internal wettability. Therefore, the degree of shrinkage was lower than that of the control group CG-0. But with the increase in GO content, the hydration rate of cement was accelerated and the autogenous shrinkage was increased. Compared with C-2 and C-5, since GO promoted hydration and increased autogenous shrinkage, while the equivalent water–binder ratio of C-5 was less than that of C-2, autogenous shrinkage decreased. From this perspective, the effect of the water–binder ratio on autogenous shrinkage is greater than that of GO content.

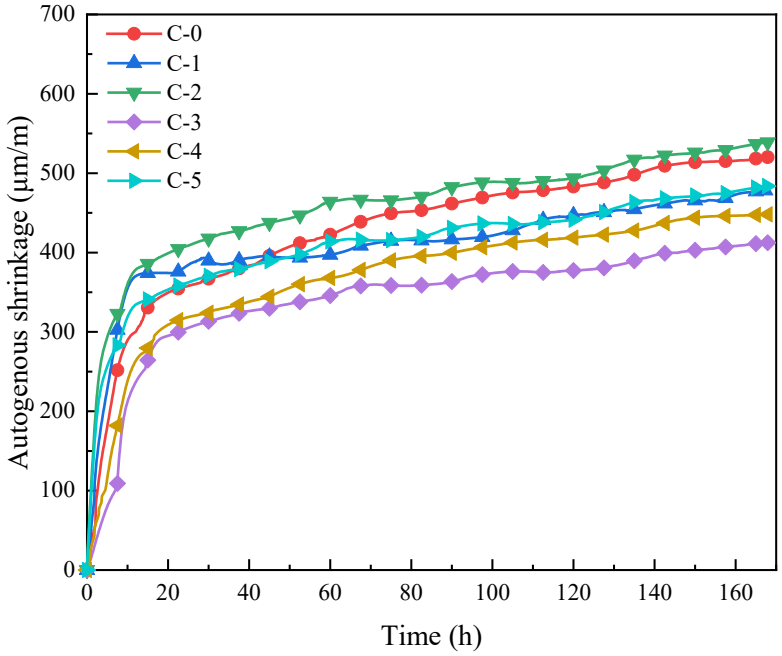


Figure 6. The influence of PCE synergistic reducing agent dispersed GO on the autogenous shrinkage of concrete.

3.3. Drying Shrinkage

Drying shrinkage refers to the evaporation of free water in the internal pores of concrete in a dry environment, resulting in an increase in the tension of capillary pores and causing shrinkage. The shrinkage of the volume will lead to the formation of microcracks inside concrete, thereby reducing its impermeability and durability. It can be observed from Figure 7 that with the increase in GO dispersion content, the development of drying shrinkage showed a downward trend. Among them, the change rate of drying shrinkage in the first 7 days was the highest, which was 505.02 μm/m, 432.08 μm/m, 401.16 μm/m and 374 μm/m, respectively, accounting for 60–70% of the total shrinkage in 56 days. With the increase in curing time, the drying shrinkage gradually decreased and tended to stabilize. According to the analysis of the effect of GO on the hydration performance of cement, it can be concluded that increasing the content of GO can promote the hydration rate of cement and accelerate the internal water consumption, resulting in a greater degree of shrinkage in the first 3 days than the blank group without GO. When the curing time was prolonged, the drying shrinkage of the mortar prepared without GO solution is the largest in the experimental group after 7 days due to its larger pore structure and faster water loss. Due to the good tensile strength of GO, the nucleation effect in cement promotes the generation of a large amount of hydration products, improves the crystal structure of hydration products, enhances its ability to resist tensile stress, and can also fill the pore cracks to refine the pore structure and reduce the porosity of cement stone. As the GO content increases, with the increase in curing time, the increase in hydration products fills a large number of pores, so that the water loss rate in the dry environment decreases, and the shrinkage pressure of capillary pores decreases, resulting in a gradual decrease in drying shrinkage.

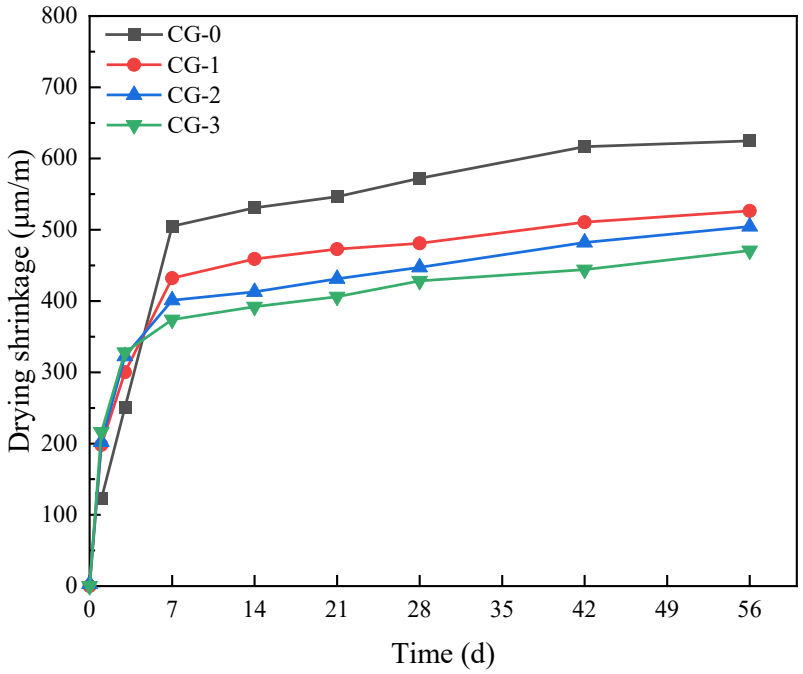


Figure 7. The influence of different GO content on the drying shrinkage of concrete.

Further analysis of the effect of GO content revealed that the drying shrinkage decreased significantly with the increase in GO content. At a GO content of 0.001% (CG-1), the 56 d drying shrinkage was 680 μm/m, representing a 17.1% reduction compared to CG-0 (820 μm/m). When the GO content is 0.003% (CG-2), the 56 d drying shrinkage value is 620 μm/m, which is 24.4% lower than that of CG-0. When the GO content is 0.005% (CG-3),

the 56 d drying shrinkage value is 580 μm/m, which is 29.3% lower than that of CG-0. The core reason for this phenomenon is the optimization of GO on the concrete microstructure: the nucleation template effect of GO can promote the generation of hydration products, refine the C-S-H gel, fill the internal pores, reduce the porosity and reduce the water evaporation channel. The high tensile strength of GO layers can enhance the tensile resistance of concrete matrix and suppress the volume deformation caused by drying. The strong binding force between GO and hydration products can also improve the compactness of the matrix and reduce the water loss in the dry environments.

As shown in Figure 8, the effect of GO co-dispersed with PCE and reducing agent on the drying shrinkage of concrete. The 3 d autogenous shrinkage of C-3, C-4 and C-5, which reduced the dosage of cementitious material, was 242.60 μm/m, 253.20 μm/m and 286.69 μm/m, respectively, significantly lower than that of the other groups. This is because the equivalent water–binder ratio of C-3, C-4 and C-5 increases, and the matrix pores contain a large amount of unreacted mixed water. The water loss rate is slower in the dry environment, resulting in smaller drying shrinkage in the first 3 days compared to that of the other groups. With the extension of curing time, the water loss rate of the sample gradually accelerated, resulting in the complete loss of water in the pores in the dry environment. The shrinkage pressure of the capillary pores increased, which was more likely to produce microcracks, so that the impermeability and corrosion resistance of the concrete decreased. The C-0, C-1 and C-2, which did not reduce the dosage of cementitious materials, generated more hydration products under the effect of GO nucleation, filled the pores and microcracks, and made the internal structure denser. In the dry environment, the water loss rate decreased, and the capillary shrinkage pressure decreased, resulting in less drying shrinkage.

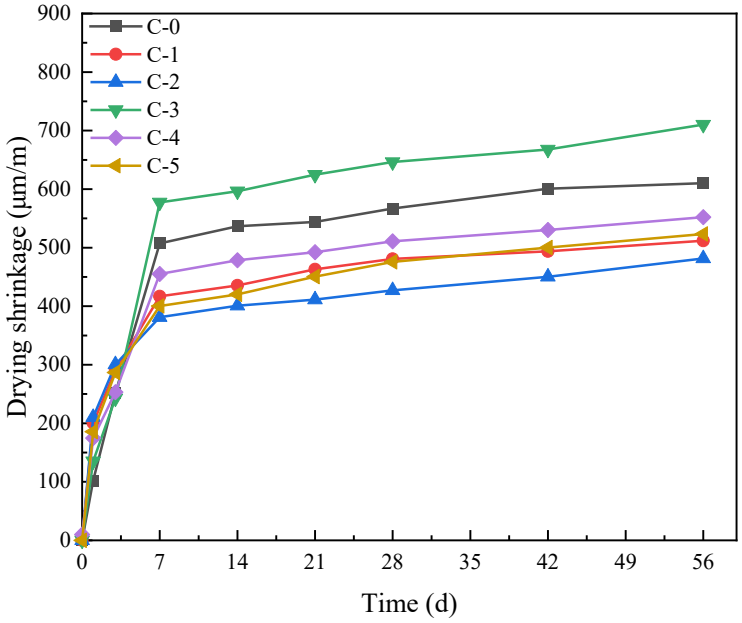


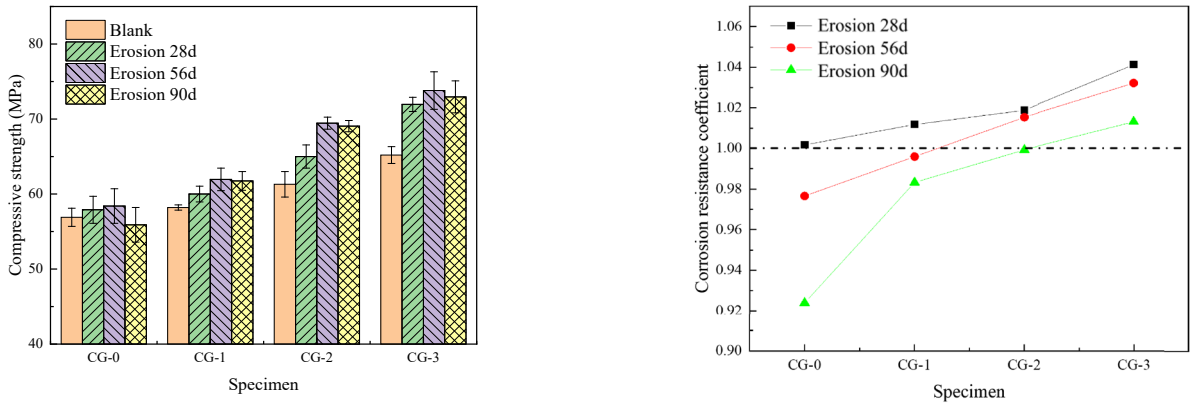
Figure 8. The influence of PCE synergistic reducing agent dispersed GO on the drying shrinkage.

It is worth noting that C-3, C-4, and C-5 have identical water–binder ratios and mixing parameters, except for the GO content. However, the shrinkage rates of C-4 and C-5 are 8.9% to 16.9% lower than that of C-3, confirming the independent shrinkage-suppressing effect of graphene oxide.

3.4. Analysis of Sulfate Resistance Performance

Sulfate corrosion of concrete structures is another major factor affecting their service life. When the concrete is located in a saline–alkali area or the sulfate concentration in the soil is too high, it will be subjected to sulfate attack, causing the concrete to expand and crack, and ultimately become a non-bonded sandstone structure, which gradually peels off from the building surface, leading to a decrease in matrix strength and service life. Corrosion resistance coefficient and compressive strength are the core indexes to evaluate the ability of sulfate resistance.

Figure 9 shows the variation curves of compressive strength and corrosion resistance coefficient of CG series concrete after soaking in sulfate solution at different ages. The control group was the specimen cured in the standard curing room for 28 days after molding. The compressive strength and corrosion resistance coefficient of the samples after 28 days of erosion showed an increase trend with the increase in GO content. In addition, the strength of all experimental groups was improved after soaking in the erosion solution for 28 and 56 days. The strength of each group was 58.4 MPa, 62.0 MPa, 69.5 MPa and 73.8 MPa, respectively. This is because the lower water–binder ratio leads to a lower degree of hydration of concrete, and its dense internal structure makes the rate of sulfate attack lower than the hydration rate. After 28 days of curing, the fly ash with pozzolanic effect began to undergo secondary hydration, and the active substance in it reacted with $Ca(OH)_2$ to form C-S-H gel, which improved the strength. The corrosion resistance coefficient of concrete decreases as erosion-time increases. When the erosion time exceeds 90 days, the strength begins to decrease, indicating that sulfate erosion has begun to play a role. The sulfate, silicate and carbonate begin to interact and consume hydration products to produce ettringite, thaumasite and other products, leading to the destruction of the concrete structures.

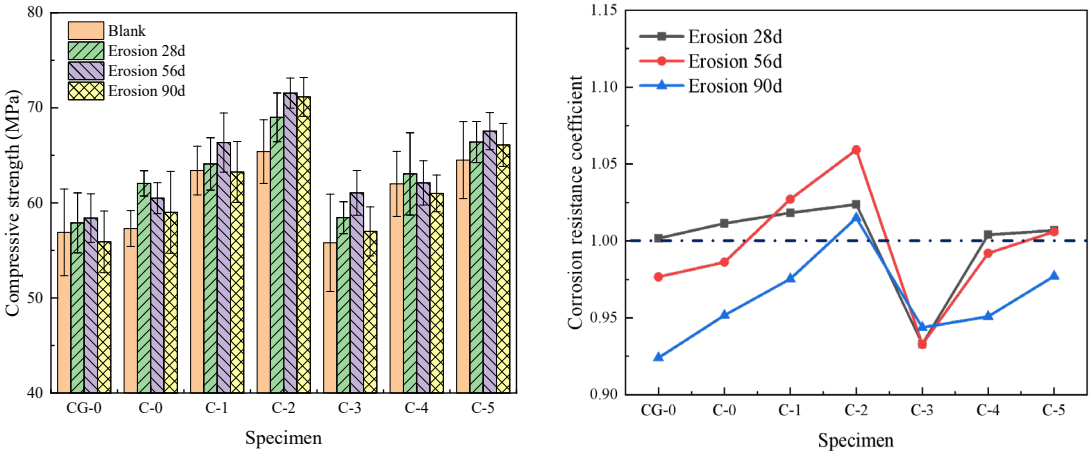


(**a**) Compressive strength. (**b**) Corrosion resistance coefficient.

Figure 9. The influence of different GO content on sulfate resistance of concrete.

As shown in Figure 10, the effect of GO solution dispersed with PCE synergistic reducing agent on the sulfate corrosion resistance of concrete is shown. From this, we can clearly find that under the same amount of gel material, with the increase in GO content, the compressive strength and corrosion resistance coefficient also gradually increase, and the strength is greater than that of GO solution separately dispersed by PCE under the same content. This is because the GO solution prepared by PCE synergistic reducing agent can be better dispersed in the cement slurry, promote cement hydration, realize the self-healing of microcracks and pores, reduce the porosity of concrete, reduce the rate of sulfate attack, and improve the durability of concrete. When the GO content was 0.003%, the 56 days sulfate attack compressive strength of C-3 was 71.6 MPa, which was 22.5% higher than

that of the control group. Because the experimental group C-3 reduced the amount of cementitious material and increased the amount of sand, the yield of hydration product C-S-H gel decreased. Although the compressive strength is improved, the slow increase in strength leads to the decrease in the corrosion resistance coefficient with the increase in erosion time.



(**a**) Compressive strength. (**b**) Corrosion resistance coefficient.

Figure 10. The influence of PCE synergistic reducing agent dispersed GO on the sulfate resistance.

3.5. Analysis of Resistance to Chloride Ion Penetration

Chloride ion penetration is the main cause of corrosion of reinforced concrete structures, and electric flux is a key index to evaluate the resistance of concrete to chloride ion penetration. All electric flux data reported in this section are the average values of three parallel specimens, ensuring the statistical reliability of the results. The chloride ion penetration resistance of concrete is divided into five grades, as shown in Table 8, and the electric flux of concrete with different strength grades needs to meet the corresponding design service life requirements, as shown in Table 9.

Table 8. Anti-chloride ion permeability grade of concrete.

Grade	Q-I	Q-II	Q-III	Q-IV	Q-V
Electric flux QS (C)	QS ≥ 4000	4000 > QS ≥ 2000	2000 > QS ≥ 1000	1000 ≥ QS > 500	QS < 500

Table 9. Electric flux and service life of concrete.

Design Service Life		100 Years	60, 30 Years
Electric flux(C) (56 d)	<C30	<2000	<2500
	C30~C45	<1500	<2000
	≥C50	<1000	<1500

As shown in Figure 11, the electric flux of CG-0 at 28 d was 1766 C and decreased to 1125 C at 56 d, with a decrease of 36.3%. Meanwhile, with the increase in GO content, the electric flux of concrete showed a gradual downward trend. When the concrete was cured to 56 d, the electric flux value decreased greatly, all lower than 1000 C. When the GO content was 0.005% (CG-3), the 28 d electric flux of concrete was 976 C, and the 56 d electric flux was 586 C, which decreased by 44.7% and 47.9%, respectively, compared with the control group. This phenomenon confirms that GO can significantly enhance the chloride ion penetration resistance of concrete. This is because the nucleation effect of GO can promote the full hydration of cement, generate more dense C-S-H gel, effectively fill

the capillary pores and harmful pores inside the concrete, reduce the porosity, refine the pore structure, and reduce the permeability of chloride ions. The two-dimensional sheet structure of GO can form a physical barrier layer in the concrete matrix. When the chloride ion migrates along the pore, the GO sheet layer will increase the tortuosity of its migration path and prolong the infiltration time. At the same time, the oxygen-containing groups on the GO surface can chemically react with the hydration products to form a stronger interfacial bonding force, improve the compactness of the interfacial transition zone, and further inhibit the penetration of chloride ions. Compared to the composite materials based on rGO reported in previous studies [26], the dual effects of chemical interfacial bonding and uniform dispersion of GO lead to lower electric flux, as the agglomeration-induced pores of rGO impair the chloride ion barrier performance.

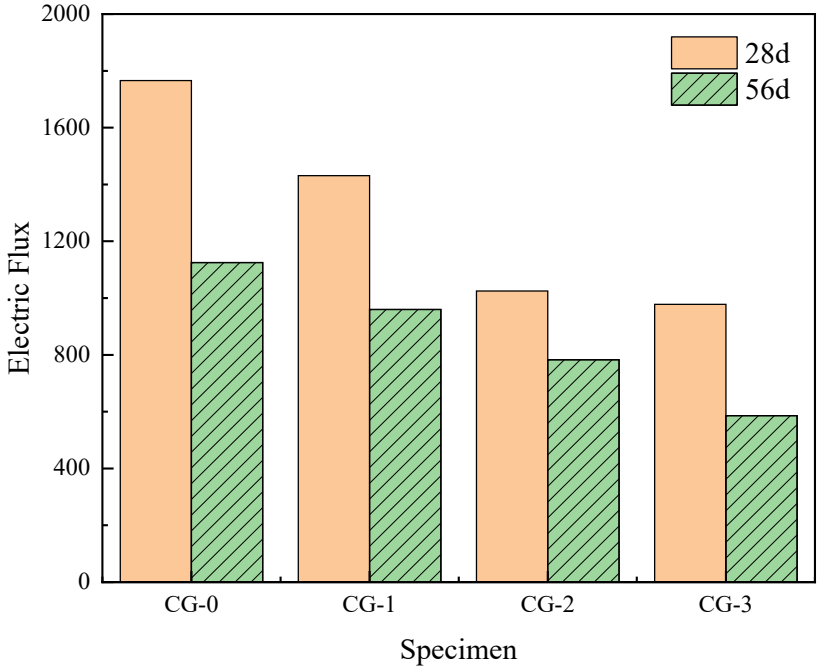


Figure 11. The influence of different GO content on the electric flux of concrete.

Combined with the analysis of Table 9, it can be concluded that the C50 concrete (≥C50) prepared in this study needs to meet a 56 day electrical flux of <1000 C in order to achieve the design service life of 100 years. CG-0 (without GO) had a 56 d electrical flux of 1125 C, slightly higher than 1000 C, and can only meet the design service life of 60 years and 30 years; the groups (CG-1, CG-2, CG-3) with GO added had a 56 day electrical flux lower than 1000 C, with CG-3 (GO content 0.005%) having the lowest electrical flux (586 C), belonging to the Q-IV level (1000 ≥ QS > 500) in Table 5, fully meeting the 100 year design service life requirement, which confirms the significant improvement effect of GO on the resistance of concrete to chloride ion penetration. It is worth noting that GO's enhancement of compressive strength here stems from the densification of microstructure, and its potential for improving tensile strength will be further explored in the subsequent research focusing on mechanical property optimization.

As shown in Figure 12, by comparing the groups without reducing the gel material (C-0, C-1, C-2) with the blank group (CG-0), it can be found that the electric flux of each group of C series was lower than that of CG-0, and it shows a downward trend with the increase in GO content. This indicates that the synergistic dispersion of GO by PCE and reducing agent can not only improve the workability, but also further optimize the pore structure of concrete and improve the resistance to chloride ion penetration. This is because the amine components in the reducing agent can be synergistically adsorbed on the surface

of the cement particles with the oxygen-containing groups on the GO surface, promoting hydration uniformity and reducing harmful pores. Comparing the groups with reduced cementitious materials (C-3, C-4, C-5) with the unreduced groups (C-0, C-1, C-2), it can be seen that under the same GO dosage, the group with reduced cementitious materials has a slightly higher electric flux. This is because after reducing the amount of cementitious materials, the equivalent water–cement ratio increases from 0.33 to 0.35, and the internal porosity of the concrete increases slightly, resulting in a decrease in chloride ion penetration resistance. However, this negative impact can be partially offset by the incorporation of GO. By comparing C-3, C-4, and C-5, it can be observed that when the water–binder ratio and other mixing parameters are the same, the flux of C-4 and C-5 decreases by 23.5–35.2%. This confirms the independent role of graphene oxide in refining the pore structure and inhibiting chloride ion penetration—a role that is independent of the influence of the water–cement ratio.

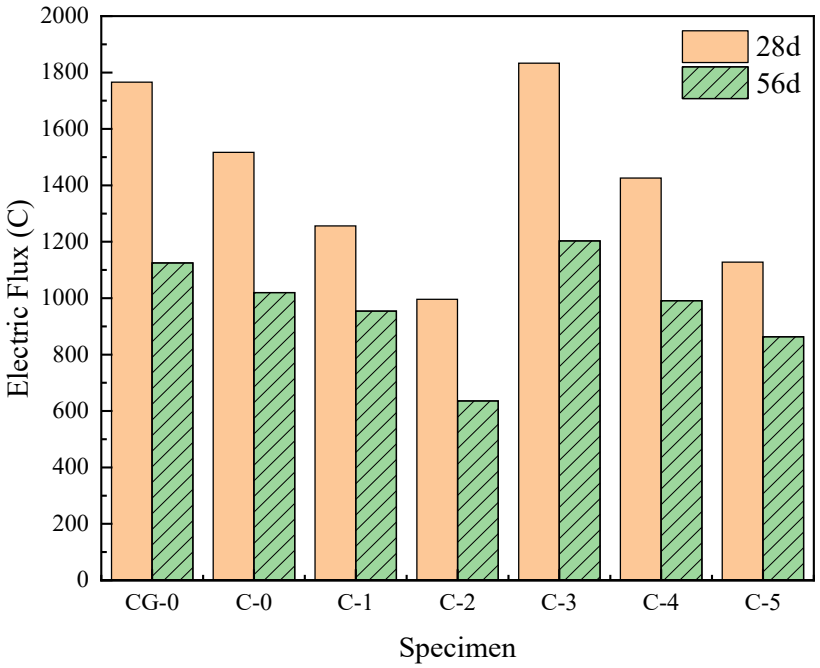


Figure 12. The influence of PCE synergistic reducing agent dispersed GO on the electric flux.

Overall, the electric flux of ordinary concrete without GO for 56 days was 1125 C, which only meets the design life of 30 to 60 years. The 56 d electric flux of the modified concrete prepared by GO is lower than 1000 C, meeting the design service life of 100 years and effectively improving the durability of concrete. Although the electric flux of concrete with single admixture of reducing agent and a decrease the amount of cementitious material has increased, its design service life still meets the requirements of 30 years to 60 years of use, which proves that the mix ratio design of compound admixture of reducing agent and GO has both economy and durability.

4. Conclusions

This study used GO dispersion to prepare modified concrete materials, and characterized their properties in terms of workability, mechanical properties, volume stability, and corrosion resistance. Through the above research, it is concluded that

(1) Slump and expansion tests revealed that GO dispersed by the synergistic combination of PCE and a viscosity reducer exhibited superior workability compared to GO modified solely with PCE. It is found that the GO dispersed by PCE and reducing agent

can improve the workability of concrete and enhance its peaceability. Mechanical property test results indicate that incorporating GO into modified concrete effectively enhances concrete strength. By adding a reducing agent, the use of cementitious materials can be reduced during the preparation of concrete.

(2) The volume stability test shows that the concrete with GO added can effectively reduce the drying shrinkage of the concrete and reduce the loss of water in the internal environment, thereby reducing the drying shrinkage of the concrete. It can also reduce the microcracks caused by the increase in capillary pressure due to drying water loss, thereby improving the durability of the concrete. Because GO has good tensile properties, can improve the crystal form of hydration products, and improve the degree of polymerization of hydration products, C-S-H gel has sufficient strength to resist shrinkage pressure, and the degree of autogenous shrinkage is decreased.

(3) The chloride ion penetration resistance test shows that when using GO to prepare modified concrete, the electric flux of concrete decreases with the increase in GO dispersion dosage. When the GO content is 0.005%, the 56 d electric flux of concrete is 586 C, which is about 50% of that of control group. This effectively reduces electric flux of concrete, improves the resistance to chloride ion erosion, and extends the service life of concrete.

(4) The results of sulfate resistance show that when GO is used to prepare modified concrete, the corrosion resistance coefficient and compressive strength increase with the increase in GO content. When the GO content is 0.005%, the sulfate resistance coefficient and strength are the highest. The modified concrete prepared by dispersing GO with PCE synergistic reducing agent shows that when the amount of cementitious material is reduced, although its strength and durability are lower than those of the experimental group without reducing the amount of cementitious material under the same conditions, its performance exceeds that of the control group, indicating the feasibility of reducing the amount of cementitious material.

Author Contributions: L.X.: Conceptualization, Methodology, Software (OriginPro 2024b (Version 10.1.5.132)), Investigation, Validation, Visualization, Formal analysis, Writing—original draft. H.W.: Conceptualization, Data curation, Methodology, Software (OriginPro 2024b (Version 10.1.5.132)). N.W.: Conceptualization. C.Z.: Conceptualization, Writing—review and editing, Supervision. X.L.: Writing—review and editing. Y.L.: Supervision. B.T.: Methodology, Conceptualization, Methodology, Supervision, Funding acquisition, Writing—review and editing. All authors have read and agreed to the published version of the manuscript.

Funding: This research received no external funding.

Data Availability Statement: Data will be made available on request. All developed codes and models supporting the findings of this study are available from the authors upon reasonable request.

Conflicts of Interest: On behalf of all authors, the corresponding author states that there is no conflict of interest.

References

1. Jibon, M.; Mahedi, M.; Yang, B.; Ceylan, H.; Cetin, B.; Bollinger, P.E.B.; Perez, M.A. Sustainable Use of Concrete Grinding Residue as a Stabilizer for Roadway Shoulder Materials. In *Proceedings of the International Conference on Airfield and Highway Pavements, Austin, TX, USA, 14–17 June 2023*; American Society of Civil Engineers: Reston, VA, USA, 2023; pp. 103–113.
2. Hou, T.; Bao, Y.; Chen, J. Mechanical-Chemical Model of Concrete Strength Under Seawater Corrosion. *Chin. Q. Mech.* **2025**, *46*, 485–497.
3. Tian, Y.; Liu, Y.; Xie, Y.M.; Zhang, G.Y.; Ye, H.L.; Yan, D.M.; Li, Y.J.; Li, B.; Xue, H.J.; Cai, Q. Coupled effects of chlorides and sulfates on steel reinforcement corrosion in concrete structures: A comprehensive review. *Case Stud. Constr. Mater.* **2025**, *22*, e04263. [CrossRef]

4. Liu, X.; Feng, P.; Chen, J.; Liu, Q.; Yu, X.H.; Cai, Y.X.; Zhu, H.; Qing, L.B.; Hong, J.X. A critical review on the interaction between calcium silicate hydrate (C-S-H) and different ions. *Constr. Build. Mater.* **2024**, *413*, 134931. [CrossRef]
5. Lu, M.; Xiao, H.; Liu, M.; Feng, J. Carbon fiber surface nano-modification and enhanced mechanical properties of fiber reinforced cementitious composites. *Constr. Build. Mater.* **2023**, *370*, 130701. [CrossRef]
6. Zhang, X.; Ji, Y.; Pel, L.; Sun, Z.; Smeulders, D. Early-age hydration and shrinkage of cement paste with coir fibers as studied by Nuclear Magnetic Resonance. *Constr. Build. Mater.* **2022**, *336*, 127460. [CrossRef]
7. Alsaif, A.; Alharbi, Y.R. Strength, durability and shrinkage behaviours of steel fiber reinforced rubberized concrete. *Constr. Build. Mater.* **2022**, *345*, 128295. [CrossRef]
8. Khalel, H.H.Z.; Khan, M.; Starr, A. Dynamic response-based crack resistance analysis of fibre reinforced concrete specimens under different temperatures and crack depths. *J. Build. Eng.* **2023**, *66*, 105865. [CrossRef]
9. Ahmed, A.A.; Shakouri, M.; Trejo, D.; Vaddey, N.P. Effect of curing temperature and water-to-cement ratio on corrosion of steel in calcium aluminate cement concrete. Constr. *Build. Mater.* **2022**, *350*, 128875. [CrossRef]
10. Chen, H.; Cao, Y.; Liu, Y.; Qin, Y.; Xia, L. Enhancing the durability of concrete in severely cold regions: Mix proportion optimization based on machine learning. *Constr. Build. Mater.* **2023**, *371*, 130644. [CrossRef]
11. He, X.J.; Zhu, E.J.; Zhang, M.X.; Wu, L.; Li, P.G. Experimental Study on Performance of High-Performance Concrete Based on Different Fine Aggregate Systems. *Buildings* **2025**, *15*, 3386. [CrossRef]
12. Yu, X.M.; Zhang, H.J.; Wang, D.H.; Ju, Y.Z.; Kang, M.X.; Ma, Y.D. Chloride Ion Penetration Resistance of Reactive Powder Concrete with Mineral Admixtures. *Mater. Sci.-Medzg.* **2024**, *30*, 233–238. [CrossRef]
13. Amran, M.; Makul, N.; Fediuk, R.; Lee, Y.H.; Vatin, N.I.; Lee, Y.Y.; Mohammed, K. Global carbon recoverability experiences from the cement industry. *Case Stud. Constr. Mater.* **2022**, *17*, e01439. [CrossRef]
14. Belaid, F. How does concrete and cement industry transformation contribute to mitigating climate change challenges? *Resour. Conserv. Recycl. Adv.* **2022**, *15*, 200084. [CrossRef]
15. Sousa, V.; Bogas, J.A. Comparison of energy consumption and carbon emissions from clinker and recycled cement production. *J. Clean. Prod.* **2021**, *306*, 127277. [CrossRef]
16. Lin, Z.J.; Lyu, G.; Fang, K.Z. Carbon emissions assessment of concrete and quantitative calculation of CO_2 reduction benefits of SCMs: A case study of C30-C80 ready-mixed concrete in China. *Case Stud. Constr. Mater.* **2025**, *22*, e04287. [CrossRef]
17. Kurmendra. Nanomaterial Gas Sensors for Biosensing Applications: A Review. *Recent Pat. Nanotechnol.* **2023**, *17*, 104–118. [CrossRef]
18. Lee, J.; Adegoke, O.; Park, E.Y. High-Performance Biosensing Systems Based on Various Nanomaterials as Signal Transducers. *Biotechnol. J.* **2019**, *14*, 18000249. [CrossRef]
19. Li, S.; Zhang, Y.; Cheng, C.; Wei, H.; Du, S.; Yan, J. Surface-treated carbon nanotubes in cement composites: Dispersion, mechanical properties and microstructure. *Constr. Build. Mater.* **2021**, *310*, 125262. [CrossRef]
20. Zhang, M.H.; Islam, J. Use of nano-silica to increase early strength and reduce setting time of concretes with high volumes of slag. *Cem. Concr. Compos.* **2012**, *34*, 650–662. [CrossRef]
21. Pan, Z.; He, L.; Qiu, L.; Korayem, A.H.; Li, G.; Zhu, J.W.; Collins, F.; Li, D.; Duan, W.H.; Wang, M.C. Mechanical properties and microstructure of a graphene oxide-cement composite. *Cem. Concr. Compos.* **2015**, *58*, 140–147. [CrossRef]
22. Kiamahalleh, M.V.; Gholampour, A.; Tran, D.N.H.; Ozbakkaloglu, T.; Losic, D. Physiochemical and mechanical properties of reduced graphene oxide-cement mortar composites: Effect of reduced graphene oxide particle size. *Constr. Build. Mater.* **2020**, *250*, 118832. [CrossRef]
23. Aretxabaleta, X.M.; López-Zorrilla, J.; Etxebarria, I.; Manzano, H. Multi-step nucleation pathway of C-S-H during cement hydration from atomistic simulations. *Nat. Commun.* **2023**, *14*, 7979. [CrossRef] [PubMed]
24. Izadifar, M.; Dolado, J.S.; Thissen, P.; Ayuela, A. Interactions between Reduced Graphene Oxide with Monomers of (Calcium) Silicate Hydrates: A First-Principles Study. *Nanomaterials* **2021**, *11*, 2248. [CrossRef] [PubMed]
25. Izadifar, M.; Dolado, J.S.; Thissen, P.; Ukrainczyk, N.; Koenders, E.; Ayuela, A. Theoretical Elastic Constants of Tobermorite Enhanced with Reduced Graphene Oxide through Hydroxyl vs Epoxy Functionalization: A First-Principles Study. *J. Phys. Chem. C* **2023**, *127*, 18117–18126. [CrossRef]
26. Zhang, N.; She, W.; Du, F.Y.; Xu, K.L. Experimental Study on Mechanical and Functional Properties of Reduced Graphene Oxide/Cement Composites. *Materials* **2020**, *13*, 3015. [CrossRef]
27. Lambert, T.N.; Chavez, C.A.; Hernandez-Sanchez, B.; Lu, P.; Bell, N.S.; Ambrosini, A.; Friedman, T.; Boyle, T.J.; Wheeler, D.R.; Huber, D.L. Synthesis and Characterization of Titania-Graphene Nanocomposites. *J. Phys. Chem. C* **2009**, *113*, 19812–19823. [CrossRef]
28. Liu, J.; Chen, S.; Liu, Y.; Zhao, B. Progress in preparation, characterization, surface functional modification of graphene oxide: A review. *J. Saudi Chem. Soc.* **2022**, *26*, 101560. [CrossRef]
29. Han, L.; Wang, X.; Xin, M.; Wang, S.; He, J. Summary of research on graphene oxide composite fiber material cement-based composites. *J. Funct. Mater.* **2024**, *55*, 3073–3082.

30. Li, Q.; He, C.; Zhou, H.; Xie, Z.; Li, D. Effects of polycarboxylate superplasticizer-modified graphene oxide on hydration characteristics and mechanical behavior of cement. *Constr. Build. Mater.* **2021**, *272*, 121904. [CrossRef]
31. Gao, Y.; Jing, H.; Chen, S.; Du, M.; Chen, W.; Duan, W. Influence of ultrasonication on the dispersion and enhancing effect of graphene oxide-carbon nanotube hybrid nanoreinforcement in cementitious composite. *Compos. Part B-Eng.* **2019**, *164*, 45–53. [CrossRef]
32. Devi, S.C.; Khan, R.A. Effect of graphene oxide on mechanical and durability performance of concrete. *J. Build. Eng.* **2020**, *27*, 101007. [CrossRef]
33. Lin, C.; Wei, W.; Hu, Y.H. Catalytic behavior of graphene oxide for cement hydration process. *J. Phys. Chem. Solids* **2016**, *89*, 128–133. [CrossRef]
34. Li, W.; Li, X.; Chen, S.; Liu, Y.; Duan, W.; Shah, S.P. Effects of graphene oxide on early-age hydration and electrical resistivity of Portland cement paste. *Constr. Build. Mater.* **2017**, *136*, 506–514. [CrossRef]
35. Lv, S.; Liu, J.; Sun, T.; Ma, Y.; Zhou, Q. Effect of GO nanosheets on shapes of cement hydration crystals and their formation process. *Constr. Build. Mater.* **2014**, *64*, 231–239. [CrossRef]
36. Stephens, C.; Brown, L.; Sanchez, F. Quantification of the re-agglomeration of carbon nanofiber aqueous dispersion in cement pastes and effect on the early age flexural response. *Carbon* **2016**, *107*, 482–500. [CrossRef]
37. Wu, L.; Liu, L.; Gao, B.; Muñoz-Carpena, R.; Zhang, M.; Chen, H.; Zhou, Z.; Wang, H. Aggregation Kinetics of Graphene Oxides in Aqueous Solutions: Experiments, Mechanisms, and Modeling. *Langmuir* **2013**, *29*, 15174–15181. [CrossRef]
38. Chowdhury, I.; Mansukhani, N.D.; Guiney, L.M.; Hersam, M.C.; Bouchard, D. Aggregation and Stability of Reduced Graphene Oxide: Complex Roles of Divalent Cations, pH, and Natural Organic Matter. *Environ. Sci. Technol.* **2015**, *49*, 10886–10893. [CrossRef]
39. Li, X.; Lu, Z.; Chuah, S.; Li, W.; Liu, Y.; Duan, W.H.; Li, Z. Effects of graphene oxide aggregates on hydration degree, sorptivity, and tensile splitting strength of cement paste. *Compos. Part A-Appl. Sci. Manuf.* **2017**, *100*, 1–8. [CrossRef]
40. Yalovega, G.E.; Brzhezinskaya, M.; Dmitriev, V.O.; Shmatko, V.A.; Ershov, I.V.; Ulyankina, A.A.; Chernysheva, D.V.; Smirnova, N.V. Interfacial Interaction in MeO_x/MWNTs (Me-Cu, Ni) Nanostructures as Efficient Electrode Materials for High-Performance Supercapacitors. *Nanomaterials* **2024**, *14*, 947. [CrossRef]
41. Wang, Y.G.; Zhong, Y.Y.; Kang, J.H.; Zhang, B.L.; Ma, Z.L.; Zhao, Q.L.; Li, J.W. Multifunctional rigid polyimide foams with outstanding EMI shielding and wave absorption via densification strategy. *J. Mater. Sci. Technol.* **2025**, *227*, 155–163. [CrossRef]
42. *GB/T 17671-2021*; Test Method of Cement Mortar Strength (ISO Method). China Building Materials Federation: Beijing, China.
43. *JGJ55-2011*; Specification for Mix Proportion Design of Ordinary Concrete. Ministry of Housing and Urban-Rural development of the People's Republic of China: Beijing, China.
44. Chen, H.T.; Sun, Z.Y.; Zhang, X.W.; Fan, J.H. Tensile Fatigue Properties of Ordinary Plain Concrete and Reinforced Concrete under Flexural Loading. *Materials* **2023**, *16*, 6447. [CrossRef]
45. Zhao, W.; Wang, R. Experimental study on the influence of high-frequency vibratory mixing on concrete performance. *Sci. Eng. Compos. Mater.* **2023**, *30*, 20220199. [CrossRef]
46. Pu, G.N.; Xiong, H.Y.; Li, N.; Liu, B. Investigation of Uniaxial Compression Stress-Strain Relationship of Early Age Manufactured Sand Concrete and Its Application. *Buildings* **2023**, *13*, 2187. [CrossRef]
47. *GB/T 50082-2024*; Standard for test methods of long-term performance and durability of concrete. Ministry of Housing and Urban-Rural development of the People's Republic of China: Beijing, China.
48. *JC/T 603-2004*; Standard Test Method for Drying Shinkage of Mortar. China Building Materials Academy: Beijing, China.
49. *GB/T50080-2016*; Standard for Test Method of Performance on Ordinary Fresh Concrete. Ministry of Housing and Urban-Rural development of the People's Republic of China: Beijing, China.

Disclaimer/Publisher's Note: The statements, opinions and data contained in all publications are solely those of the individual author(s) and contributor(s) and not of MDPI and/or the editor(s). MDPI and/or the editor(s) disclaim responsibility for any injury to people or property resulting from any ideas, methods, instructions or products referred to in the content.